

Multilateral Sound Manipulation Using Magnetically Tunable Apertures

Shubhi Bansal,* Christabel Choi, and Sriram Subramanian

In recent years, planar aperture-based acoustic devices have been investigated due to their thin form factor, high effective transmission, and sound modulation capability. Moreover, reconfigurable and tunable devices are being continuously researched to enable multiple degrees of freedom in real time. Herein, an aperture-based acoustic device is presented, which enables tunable multilateral ultrasonic operation. Sound waves are manipulated in multiple directions by continuously tuning aperture width or length, using a magnetically controlled rod. The position, orientation, and geometrical properties of the rod (i.e., length, topographical curvature) are exploited to create a varied interface for the impinging sound. Through experiments and simulations, acoustic wave steering in different orthogonal planes and acoustic switching using a single tunable device unit are demonstrated. Furthermore, different four-unit device configurations are implemented for tunable beam-formation and tunable acoustic focusing applications by utilizing the acoustic anisotropy of the system. The tunable dynamic acoustic device is scalable to audible frequencies and enables tilted operation. This straightforward and accessible proof-of-concept opens a paradigm for exploring multifunctional aperture-based designs with greater degrees of freedom, bringing us a step closer toward practical applications such as acoustic device integration with walls, window panels, and other commercial products for tunable sound transmission.

1. Introduction


Tunable acoustic wave manipulation is a well-researched problem that has seen recent developments using various acoustic devices, such as phononic crystals,^[1] reconfigurable acoustic metamaterials,^[2–4] or dynamic acoustic phased arrays^[5,6] to achieve applications like frequency-selective wave beaming,^[7] acoustic wave steering,^[8] and numerous other holographic applications.^[6] In the last decade, continuous research efforts have been made to design and develop active designs,^[9,10] which

may utilize control mechanisms like mechanical, heat, or electric control, for attaining structural variation to allow dynamic sound modulation.^[11] Dynamic sound modulation allows modulation of the output sound field in real time and on-demand, without modifying the input. For instance, controlled structural variation has been recently reported for an origami-based acoustic Helmholtz resonator with a dynamic cavity, which was demonstrated using real-time pneumatic control for broadband sound attenuation.^[12] Dynamic sound modulation enables multifunctional operation, which is a capability that brings us closer toward achieving real-life applications, which often require versatile operation in a frequently changing environment.

While phased arrays are powerful acoustic devices for dynamic sound modulation, they come with the challenges of the need for precise calibration, the high cost of hardware, aliasing effects, and electronic control complexity.^[2,13] Alternatively, other acoustic devices such as metamaterials have emerged to enable a myriad of applications such as lensing, energy harvesting,

near-perfect absorption, and beam focusing.^[14–17] Different designs of acoustic devices have been developed^[18,19] such as labyrinth structures,^[20,21] Helmholtz resonators,^[22–25] and multi-apertures,^[26,27] and some are even compatible with phased arrays.^[3,28] In particular, planar aperture-based acoustic devices have proven to be effective sound manipulation devices while retaining a thin form factor (often of subwavelength thickness), which is appealing for future integration with commercial applications.^[8–10] Transmissive and attenuating sound effects have been previously observed in such aperture arrays. Extraordinary acoustic transmission (EAT)^[29] through an array of subwavelength apertures (a periodic grating^[30]) within a fluid was experimentally found to be a result of excited surface diffractive waves and Fabry–Pérot resonant modes within the apertures. EAT has continued to be an area of interest, where devices with holes or apertures within rigid substrates have demonstrated the enhancement of acoustic subwavelength imaging resolution.^[31,32] Similarly, it has been observed that ultrasound could be shielded much more effectively by using perforated metal films in water than uniform surfaces at certain wavelengths, resulting in extraordinary acoustic screening.^[33] However, there are few aperture-based acoustic devices which can be actively reconfigured to enable multiple modes of operation in real time.

S. Bansal, C. Choi, S. Subramanian
Department of Computer Science
University College London
London WC1E 6BT, UK
E-mail: shubhi.bansal@ucl.ac.uk

 The ORCID identification number(s) for the author(s) of this article can be found under <https://doi.org/10.1002/adem.202301339>.

© 2024 The Authors. Advanced Engineering Materials published by Wiley-VCH GmbH. This is an open access article under the terms of the Creative Commons Attribution License, which permits use, distribution and reproduction in any medium, provided the original work is properly cited.

DOI: 10.1002/adem.202301339

In this work, we develop a magnetically actuated aperture-based acoustic device capable of on-demand multilateral control. Our acoustic device allows dynamically tunable sound transmission without using any power or electricity. It can manipulate sound waves in multiple directions in 3D space using only a single aperture and a single transducer as a source. Generally, directional wave manipulation is not possible with a single transducer alone. Given a row of transducers (e.g., 1D phased array), wave steering can mostly be implemented in a single plane. A phased array of transducers can allow for multilateral sound control if it is large enough, but a greater degree of computational and electronic complexity would be required, and it would suffer from aliasing effects. Moreover, it is more expensive to operate. Our approach, on the other hand, is cost-effective while providing the required acoustic pressure distributions.

Recently, active control of a large aperture through a domestic window was reported to reduce broadband (100 Hz to 1 kHz) sound, and attenuation of -10 dB was achieved for urban transportation noise.^[34] Although the aim of that work was to solve the problems associated with closing a window to reduce noise, it highlighted the effectiveness of sliding a window or aperture shut. Similarly, a microfluidic acoustic metamaterial was proposed to tune the transmitting sound field over a broadband range using dynamic liquid droplet motion over an aperture,^[4] and dynamic acoustic levitation was achieved using a reflector plate with 12 tunable circular apertures.^[35] Utilizing the similar principle of adjusting a camera shutter to reduce the amount of light entering a lens or rolling up blinds to brighten up a room, here, we modulate the transmitted sound by physically placing an object at the surface of a single aperture.

To control the size of the aperture, we use a cylindrical rod. For our application, a cylindrical geometry has two features of interest: 1) curvature^[36] and 2) anisotropy.^[37,38] Curved surfaces strongly influence the incident sound field, as seen by reflection, divergence, and scattering phenomena of sound waves explored in the literature.^[39] The curvature is determined by the diameter of the cylinder. The length of the cylinder determines the available curved surface area, which can be used to interact with the sound. In this work, the aperture has a base shape of a rectangle. Depending on the location or orientation of the cylindrical rod on the rectangular aperture, the size of the open aperture would vary in different orthogonal planes, enabling an anisotropic sound response. Hence, without changing the structure of the physical obstacle, multiple multilateral acoustic outputs are achievable.

To demonstrate this acoustic modulation mechanism, we use magnetic actuation. The cylindrical rod is fabricated with magnetic silicone rubber (i.e., magnetorheological elastomer).^[3,40,41] By embedding magnetic particles within the silicone matrix, the cylinder is able to move and respond to external magnetic fields. When controlled by a magnet, the rod can be rolled continuously along the aperture in different orientations and positions to modulate the sound in real time, i.e., enabling dynamic sound modulation. In the chosen rod orientation, the rod can also be stopped at any position along the slit to maintain the desired modulated output sound field. No source of power or electricity is required to maintain rod's static state. Our magnetic control mechanism is especially advantageous for tunable operation in the ultrasonic regime (>20 kHz), where the working wavelength is small (few millimeters), thus, manually repositioning the

small cylindrical rod (1 mm radius ($\approx\lambda/8$)) is challenging for modulating the sound field. To date, there has been no previous attempt to demonstrate multilateral sound control with a single aperture via magnetic actuation.

Both numerically and experimentally, we demonstrate multiple acoustic functionalities in different orthogonal planes. Functionalities include acoustic wave modulation, wave steering, and acoustic switching, using a single rod and aperture device unit. Thereafter, we explore two symmetric multiaperture configurations composed of four device units. Here, the multilateral functionality of the rod and aperture units are utilized and configured into functional arrays to demonstrate tunable beam formation and tunable near-field focusing for acoustic pressure modulation. The proposed acoustic device is easy to replicate, uses easily accessible and low-cost materials for fabrication, and is applicable for implementation on a larger scale. The transmissive design of our device differs from reflective designs^[2,42] which require the input source waves to be on the same side as the output for operation. This transmissive characteristic could simplify integration with commercial devices, where it could potentially be part of a thin partition or window. Our experimental demonstrations in this work operate at 40 kHz, thereby opening potential ultrasound applications, such as integration with commercial devices that utilize ultrasound frequencies for mid-air haptics,^[43,44] acoustophoretic volumetric images,^[6] or energy harvesting.^[17] It is also possible to scale the acoustic device to lower frequencies for implementation with larger wavelengths. This could enable real-life audible sound applications, compatible with sound-based furniture and architectural designs.

2. Design Concept

We fabricated a rectangular aperture (subwavelength dimensions, 4.5 mm \times 0.5 mm) on a transparent polyethylene terephthalate (PET) substrate (thickness ≈ 0.2 mm) as our device base structure (Figure 1a). Using 40 kHz ultrasound, we investigated different configurations of the cylindrical rod over the aperture, namely, when the rod is parallel (PAR) to the aperture (Movie S1, Supporting Information), perpendicular (PER) to the aperture (Movie S2, Supporting Information), and with different degrees of coverage, i.e., fully covered (Figure 1b) or partially covered (Figure 1c) (Movie S3, Supporting Information). The point (in red) at the center of the aperture and the point (in red) where the rod is in contact with the substrate (i.e., the point of contact where the normal passes through center of the circular cross section of the rod) are taken as reference points. The distances between them are defined as either d_w or d_l , depending on the orientation of the rod, to tune either the width or length of the aperture (Figure 1d). Here, we used a rod with an approximate length of 8 mm and radius of 1 mm (Figure S1, Supporting Information). The cylindrical rod was actuated and moved in real time over the rectangular aperture using an external magnetic stimulus, i.e., a permanent magnet, to manipulate the acoustic output. To ensure that the actuating magnet does not interfere with the aperture, actuation was implemented from the side of the aperture. A thin piece of wire (0.6 mm diameter) was inserted through the center of the main magnetic rod, and the other end of the wire was inserted into a

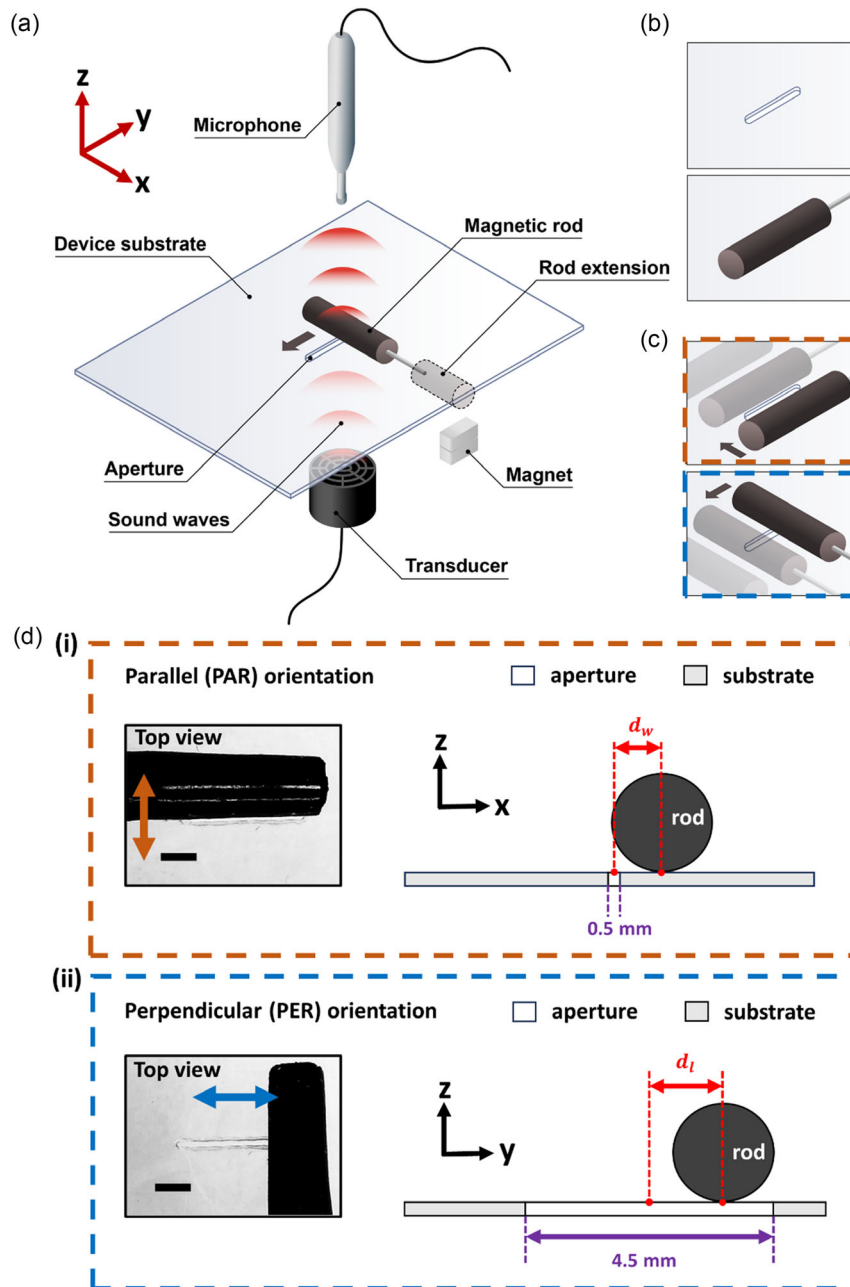


Figure 1. a) Schematic representation of the experimental setup. The acoustic transducer was placed directly below the substrate (2 mm gap), producing ultrasonic 40 kHz waves. The received output was measured at 10 mm ($\approx 1.2\lambda$) above the substrate. A cylindrical magnetic silicone rod was placed over the aperture to tune the transmitting sound field. Schematics of different cylinder orientations to manipulate the transmitting sound field through the aperture, namely, b) open aperture (top) and fully covered (bottom), and c) partially covered apertures in PAR (top, dotted orange border) and PER (bottom, dotted blue border) orientations. Movement of rod shown by black arrows. d) Partially covered orientations according to the orange and blue dotted borders in (c). i) Top view experimental photograph of the PAR orientation, with orange arrows indicating direction of actuation. Scale bar, 1 mm. On the right, a schematic of the cross-sectional side view. The distance between the center of the width of the aperture, to the normal of the circular cross section of the rod PER to the substrate, is defined as d_w (in red). The width of the aperture is shown in purple. ii) Top view experimental photograph of the PER orientation, with blue arrows indicating direction of actuation. Scale bar, 1 mm. On the right, a schematic of the cross-sectional side view. The distance between the center of the length of the aperture, to the normal of the circular cross section of the rod PER to the substrate, is defined as d_l (in red). The length of the aperture is shown in purple.

smaller magnetic cylinder, away from the aperture. The smaller cylinder had a magnet below it to move and tune the position of the rod on the aperture. Magnetic actuation and control were also well aligned without the rod slipping when the PET substrate was tilted, upright, or positioned upside down (Figure S2, Supporting Information), making it potentially suitable for future real-life commercial applications like parametric audio devices.

3. Results

In this section, we present tunable acoustic operations using our dynamic acoustic device such as tunable acoustic switching, acoustic wave steering, beam formation, and near-field acoustic focusing. Acoustic simulations for our device were carried out in the numerical simulation software COMSOL Multiphysics, Version 6.1. (details in Experimental Section). We used the acoustic pressure frequency domain model physics to simulate the acoustic wave behavior and obtain the acoustic output according to the position of the rod on the aperture. However, we did not account for the magnetic actuation in the simulations because we wanted to simulate and capture the functionally modified acoustic field after the rod has been actuated and moved to a desired aperture position. The simulations were modeled after the experimental setup as shown in Figure S3, Supporting Information, and depicted schematically in Figure 1a.

3.1. Acoustic Switch

To tune the impinging sound waves, we completely covered the aperture in the PET substrate using magnetic rod which contributed to the high impedance contrast with the air surrounding the aperture. **Figure 2** shows the acoustic pressure measurements and simulations for an open aperture, and when the aperture was fully covered and closed by the rod. The aperture was fully covered by placing the rod in a PAR orientation, where the width of the rod (2 mm) is 4 times the width of the aperture (0.5 mm). When covered by the rod, the transmitted sound output decreases. Compared to the open aperture, we measured an experimental drop in pressure of 31.9 dB and simulated a drop of 23.9 dB between the two states. These values were recorded based on a horizontal cutline taken around the center of the aperture. The discrepancy between experiments and simulations is attributed to experimental losses due to air viscosity and reflection from the experimental setup (tables or support structures), which are not accounted for in simulations. We, therefore, successfully demonstrated acoustic switching with distinct high and low states.

3.2. Acoustic Wave Steering Using a Partially Covered Single Aperture Unit

In a PAR orientation, the rod was shifted from the center (fully covered position shown in Figure 2) of the aperture toward the right and left positions by $d_w = \pm 0.75$ mm. We measured and simulated the modulated acoustic pressure amplitude in the XY plane, which demonstrated the directional propagation of the steered acoustic waves (**Figure 3**). When the aperture was completely unblocked, the acoustic pressure was concentrated at the center of the aperture. From the center of the aperture,

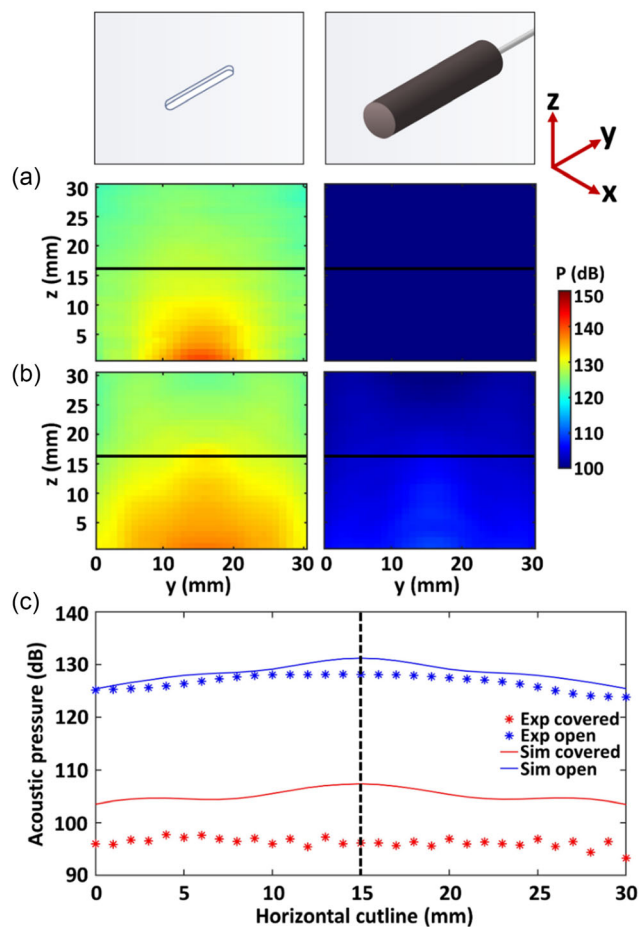


Figure 2. a) Experimental and b) simulated acoustic pressure (dB) plots in the YZ plane, showing sound switching with an open aperture (left), and fully covered aperture in a PAR orientation (right). Corresponding schematics are in the top row. c) Simulated and experimental line plots, where acoustic pressure (dB) is plotted against a horizontal cutline (30 mm) taken approximately 26 mm (3λ) above the aperture (solid black lines in (a) and (b)). Simulated results are plotted with solid lines, and experimental results are plotted with markers. Lines for the fully covered aperture are shown in red, and lines for the open aperture are shown in blue. The vertical black dotted line marks the center of the aperture.

the rod was moved on the right edge of the aperture and the acoustic pressure was concentrated toward the left side of the XY plane (Figure 3b). Similarly, when the rod was moved gradually from the center to the left edge of the aperture, the acoustic field propagated toward the right side of the XY plane (Figure 3c).

In **Figure 4a**, we plot the transmitted acoustic pressure for the PAR orientation against a horizontal cutline of 50 mm, along the x -axis. The cutline is positioned directly 26 mm (3λ) above the aperture. The 25 mm mark along the cutline corresponds to the center of the aperture. As the acoustic wave steers toward the left, the acoustic pressure drops along the cutline. At $x = 10$ mm, the simulated amplitude is 130 dB when the aperture is partially covered. This is higher than the amplitude when the aperture is open (126.7 dB), indicating a concentration of pressure of the steered acoustic waves. For the partially

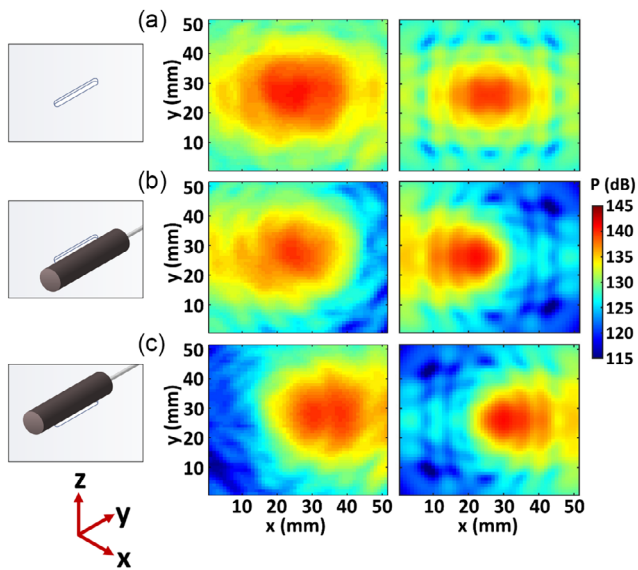


Figure 3. Experimental (middle column) and simulated (right column) acoustic pressure plots (dB) taken in the XY plane for a) an open aperture, b) partial coverage ($d_w = +0.75$ mm) of the aperture by the rod in a PAR orientation along the right long aperture edge, and c) partial coverage ($d_w = -0.75$ mm) of the aperture by the rod in a PAR orientation along the left long aperture edge. Corresponding schematics are in the leftmost column.

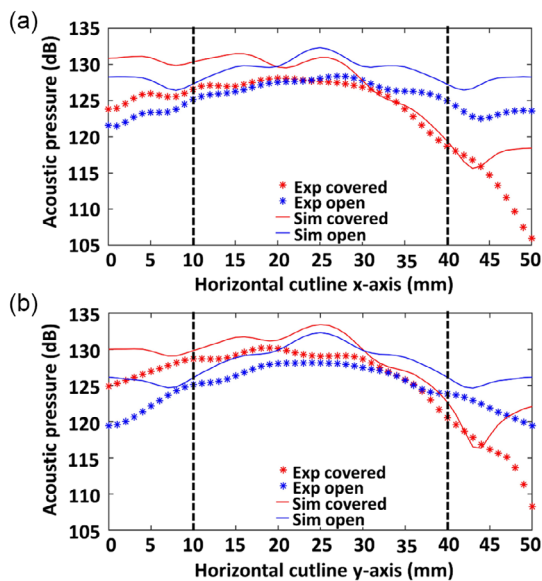


Figure 4. Acoustic pressure amplitude line plots (dB) taken against a horizontal cutline (50 mm) positioned 26 mm (3λ) above the center of the aperture along the a) x-axis, for the PAR orientation with partial coverage ($d_w = +0.75$ mm), and along the b) y-axis for the PER orientation with partial coverage ($d_l = +2$ mm). Simulated results are plotted with solid lines, and experimental results are plotted with markers. Pressure lines for the partially covered aperture are shown in red, and pressure lines for the open aperture are shown in blue. The vertical black dotted lines mark the locations ± 15 mm from the center of the aperture at $x = 25$ mm.

covered case, at $x = 40$ mm, the acoustic pressure decreases by 9.3 dB, to 120.7 dB.

These simulated results are validated by experiments. The experimental values exhibit the same behavior, where the acoustic pressure for the partially covered case starts off higher than the open case and drops in the region where the acoustic waves are steering away from. At $x = 10$ mm, the measured amplitude is 126 dB when the aperture is partially covered, higher than the amplitude when the aperture is open (124.5 dB). For the partially covered case, at $x = 40$ mm, the acoustic pressure decreases by 6.5 dB, to 119.5 dB.

We observe results similar to Figure 4a as plotted in Figure 4b for the PER case, but in a different plane of measurement. Here, the cutline was instead plotted along the y-axis. As the acoustic wave steers toward the left, the acoustic pressure drops along the right of the cutline. At $y = 10$ mm, the simulated amplitude is 129.4 dB when the aperture is partially covered. This is higher than the amplitude when the aperture is open (125.4 dB), once again illustrating that the pressure of the acoustic waves is higher toward the left. For the partially covered case, at $y = 40$ mm, the acoustic pressure decreases by 5.4 dB, to 124 dB. In comparison, for the experiments, at $y = 10$ mm, the measured amplitude is 128.5 dB for the partially covered aperture and 124.8 dB for the open aperture. For the partially covered case, at $x = 40$ mm, the acoustic pressure decreases by 6.8 dB, to 121.7 dB.

Acoustic wave steering was only observed in the orthogonal plane PER to the orientation of the rod in both the PAR and PER cases (Figure 5). For the measurement plane PAR to the rod, the wave fronts are observed to not steer or propagate asymmetrically, contributing to the anisotropy of the setup. When the rod was in the PER orientation, only the length of the long edge

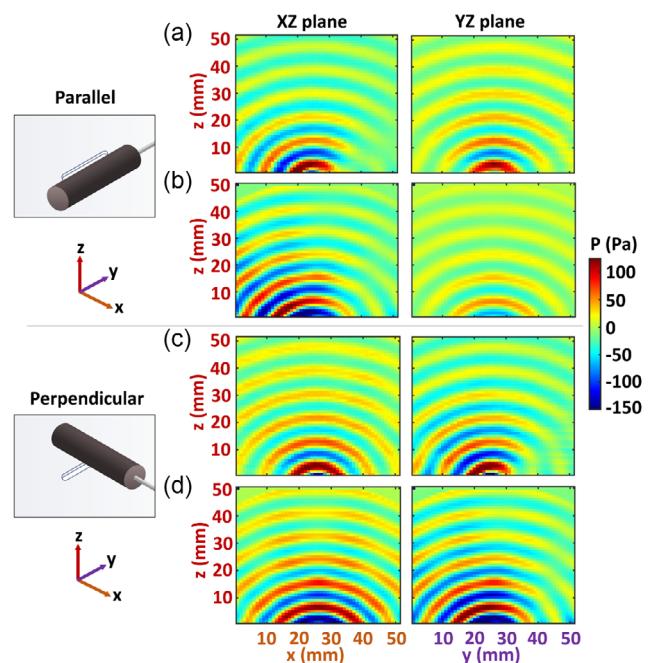


Figure 5. Anisotropic sound modulation in orthogonal planes. Experimental a,c) and simulated b,d) total acoustic pressure (Pa) plots in both the XZ (middle column) and YZ (right column) planes. The corresponding schematics are shown on the left.

was being tuned to change the size of the aperture. In this case, the curvature and position of the rod did not interfere with the geometry of the aperture with respect to the short edge. Thus, the transmitting sound field in the plane PAR to the rod, i.e., the XZ plane, did not show any acoustic wave steering

Based on the results for acoustic wave steering, we observe acoustic anisotropy where the transmitting wave is modulated and steered in a measurement plane PER to the rod, while it remains unsteered in the measurement plane PAR to the rod. To validate this, we made a further comparison of simulated and experimental results in the XZ plane (PAR to the orientation of the rod), with the partially covered and open aperture. As shown in Figure 6, we did not observe any steering in the XZ plane, and

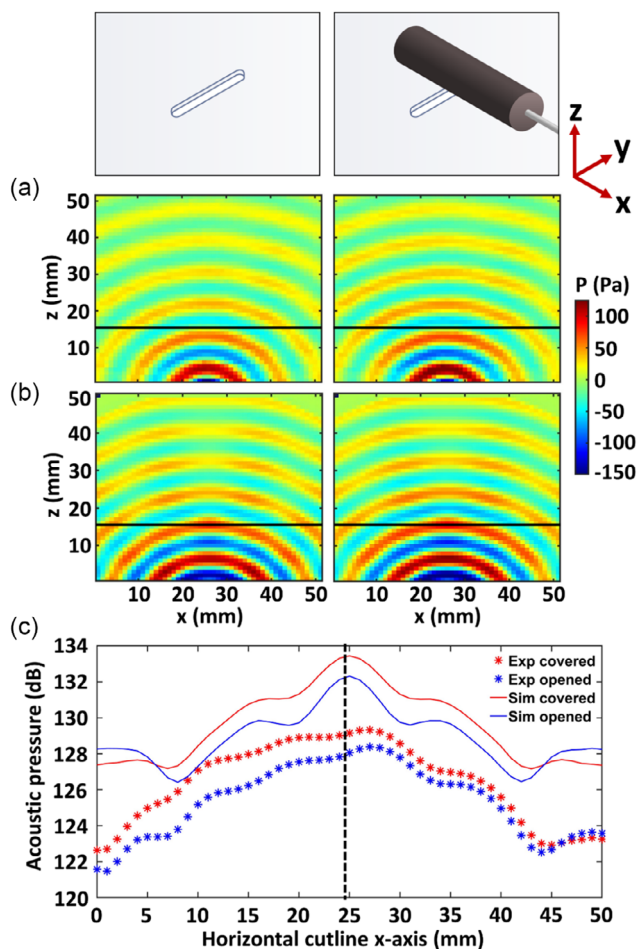


Figure 6. a) Experimental and b) Simulated total acoustic pressure (Pa) plots in the XZ plane which is PAR to the orientation of the rod. The corresponding schematics are shown in the top row, and the left column shows results for an open aperture, and the right column is for the partially covered ($d_i = +2$ mm) aperture by the rod in a PER orientation along the right short aperture edge. c) Simulated and experimental line plots, where acoustic pressure (dB) is plotted against a horizontal cutline (50 mm length) taken approximately 26 mm (3λ) above the aperture (marked by solid black lines in (a) and (b)). Simulated results are plotted with solid lines, and experimental results are plotted with markers. Lines for the fully covered aperture are shown in red, and lines for the open aperture are shown in blue. The vertical black dotted line marks the center of the aperture.

the transmitted total acoustic pressure was enhanced when the length of the open aperture was reduced (by placing rod), which matches well with the simulated results. This behavior could be attributed to the EAT^[29,30] reported in the literature but it will require further investigation in the future.

3.3. Tunable Beam Formation with Multiple Apertures

Acoustic devices that can be continuously tuned have the ability to generate sound radiation patterns in a desired shape on-demand. By patterning our acoustic device into an array, i.e., a single rod and aperture, it is possible to create a customized acoustic output. Here, we demonstrate this numerically using arrays consisting of four rods and aperture units in two different configurations, utilizing the PAR and PER orientations, respectively. We further explore how system anisotropy can be functionally applied for applications in tunable acoustic beam formation and near-field acoustic pressure focusing.

3.3.1. Four Aperture and Rod Units in PAR Orientation for Tunable Beam Formation

Here, four apertures are positioned adjacent to one another at right angles, forming the edges of a square (Figure 7a). On each of the apertures, a rod is placed in the PAR orientation for tuning the open aperture width. The distance between each two opposing PAR apertures from center to center is 6 mm. To evaluate the effectiveness of the designed acoustic device array in tuning the transmitting sound beam, we conducted numerical simulations using COMSOL Multiphysics, Version 6.1, with the in-built parametric sweep function. The main parameter in the sweep was d_w , which is the distance of the center of the rod to center of width of the aperture (explained in previous section) over a range of five points from 0.5 to 0.1 mm, with decrements in step sizes of 0.1 mm. We did not use step sizes smaller than 0.1 mm, considering the possible feasibility of practical implementation with our current magnetic actuation method. Following the single aperture simulations, we applied the pressure acoustics model to the current setup. An outer spherical geometry of air was applied to the setup, along with an outermost perfectly matched layer (PML) boundary to minimize wave reflections (Figure S4, Supporting Information). The single transducer source (10 mm diameter) was placed at the center of the substrate, 2 mm below it. The rod dimensions were subwavelength, i.e., 1 mm radius as with previous sections; however, the length of the rod was chosen to be 5 mm, so that all four rods and apertures stayed within the transducer domain. Figure 7b shows the pressure map distribution for when all four apertures are completely open (left graph) and when $d_w = 0.2$ mm (right graph). Figure 7c graphically illustrates the effect of moving the rods over the apertures to tune d_w from 0.5 to 0.1 mm and when the apertures were completely open. Thus, we tuned the maximum absolute beam pressure (based on the horizontal cutline) from 270 to 165 Pa, with the uncovered case giving a pressure of 325 Pa. With each movement of rod, for a step size of 0.1 mm, the sound pressure decreased by 26.3 ± 3.66 Pa. The results clearly demonstrate that as the aperture coverage increases, the transmitting acoustic pressure decreases, which

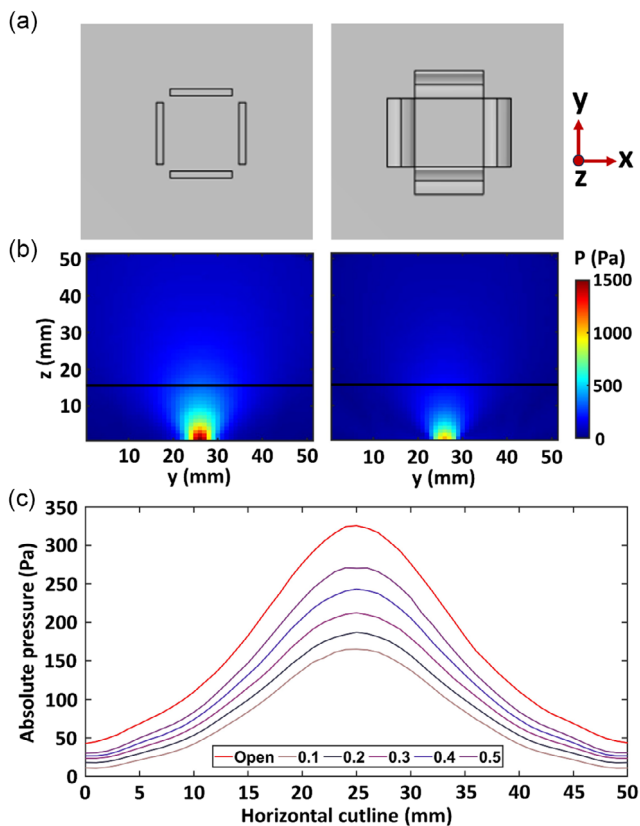


Figure 7. a) COMSOL Multiphysics images of four open apertures (left), and four apertures with partial coverage from the rods in the PAR orientation where $d_w = 0.2$ mm (right). b) Corresponding simulated absolute acoustic pressure (Pa) maps in the YZ plane. c) Simulated absolute acoustic pressure (Pa) line plots according to the coverage of the aperture using the rod, plotted against a horizontal cutline (50 mm) taken approximately 16 mm ($\approx 2\lambda$) above the aperture (marked by solid black lines in (b)) in the YZ plane.

is attributed to the decrease in open aperture width. Hence, this four-unit configuration can be used for tuned attenuation of the propagating sound beam.

3.3.2. Four Aperture and Rod Units in PER Orientation for Tunable near-Field Acoustic Focusing

Here, the four apertures are positioned PER to one another forming a “plus” or “cross” shape (Figure 8a). On each of the 4.5 mm long apertures, a 5 mm long rod is placed in the PER orientation. The distance between two opposing apertures from center to center is 6 mm. In this application, the rods have a larger cross-sectional circular radius of 2 mm to cover a larger area on the aperture length (4.5 mm). The rods also have a shorter length of 5 mm to prevent them from obstructing one another. We used the same numerical simulation in COMSOL Multiphysics, Version 6.1, similar to the section above, applying the pressure acoustics, frequency domain module physics to simulate near-field focusing. The main parameter in the sweep was d_1 , which is the distance of the center of the rod from center of

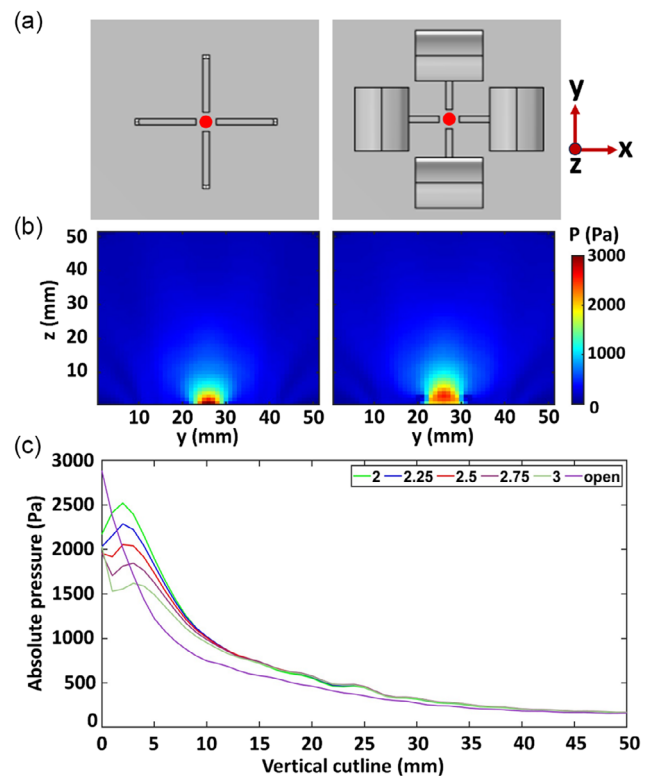


Figure 8. a) COMSOL Multiphysics images of four open apertures (left) and four apertures with the partially covering rods in the PER orientation where $d_1 = 2$ mm (right). b) Corresponding simulated absolute acoustic pressure (Pa) plots in the YZ plane. c) Simulated line plot according to the partial coverage of the apertures by moving the rods from 3 to 2 mm in steps of 0.25 mm, where absolute acoustic pressure (Pa) is plotted against a vertical cutline (50 mm) taken at the center of the YZ plots, where $\gamma = 25$ mm. The vertical cutline is marked as the out of the plane point shown by the red circular markers in the COMSOL images in (a).

length of aperture (explained in previous section), over five points from 3 to 2 mm, with decrements of 0.25 mm. Figure 8b shows the pressure map distribution for when all four apertures were completely open (left graph) and when $d_1 = 2$ mm (right graph). Figure 8c graphically illustrates the effect of moving the rods over the apertures to tune d_1 from 3 to 2 mm and when the apertures were completely uncovered. According to the vertical cutline positioned at the center of the four units in the YZ plane, we achieved near-field acoustic focusing for the transmitting sound field. Thus, we tuned the maximum absolute pressure at the focal points (based on the vertical cutline) from 1618.9 to 2521.8 Pa. With each step size of 0.25 mm, the sound pressure increased by 235.7 ± 23.79 Pa. The results clearly demonstrate that with greater coverage of the open aperture by the rod, the focused acoustic pressure increases and the focal peak shifts toward the device substrate in the z -direction. In addition, at a greater distance along the vertical cutline points in Figure 8c, i.e., beyond the near field, the partially covered aperture configuration continued to give a higher output than the uncovered open aperture configuration. Hence, this four-unit configuration can be used for tuned focusing and enhancement of the propagating sound waves.

4. Discussion and Outlook

We successfully designed and implemented a dynamically tunable acoustic device, where each unit consisted of a cylindrical magnetic obstacle, employed to tune an open aperture in real time. A main contribution of this work was the approach of exploiting the geometric relationship between the cylindrical rod and the aperture to manipulate the transmitting sound in different orthogonal planes. Without any modification to the geometry of the rod or aperture components in isolation, we utilized facile changes in their orientation and position to controllably alter the sound field in 3D space. Tuning the length and width dimensions of the single aperture allowed the sound waves to be directed multilaterally, i.e., different directions along the four aperture edges. Compared to other rod geometries such as a hemisphere or a cube, the advantage of a cylindrical geometry was the lack of sharp corners and a constant curvature across the entire length of the rod. For instance, if a sphere was instead used for partial coverage and positioned PAR to the long edge of the aperture, the coverage of the sphere would have been non-uniform and reduced at the edges.

Our single acoustic device unit, of subwavelength dimensions, was operational at an ultrasonic frequency of 40 kHz and capable of multiple functionalities like switching and wave steering, both shown through simulations and experiments. It is noteworthy that acoustic wave steering is a functionality which usually requires an array of multiple units,^[45–48] and has never been reported previously with the use of a single acoustic device unit. First, we started with a PAR orientation, where the rod was placed PAR to the length of aperture to tune the width of the aperture. We demonstrated the functionality of acoustic switching, where we achieved a difference of 20–30 dB, with and without the rod covering the aperture. Thereafter, we moved the rod across the full aperture from the long right edge to the long left edge. Accordingly, as the aperture was tuned, the propagated acoustic waves were directed from left to right. These results were captured in two measurement planes (XY and XZ), indicating a functionality of acoustic wave steering. We repeated the experiments in the PER orientation, where the rod was PER to the aperture length, to tune the length of the aperture. Once again, we observed acoustic wave steering, but instead in the YZ plane and not in the XZ plane. Both simulated and experimental results were in good agreement and validated the acoustic anisotropy of the setup. Acoustic wave steering was only seen in the planes PER to the orientation of the rod; while in the corresponding orthogonal plane PAR to the rod, there was no steering. Our results for a single rod and aperture unit demonstrated the versatility of the setup, allowing for multiple degrees of freedom through controllable variations in the positioning and orientation of the rod and aperture components. Moreover, our acoustic device unit is easy to replicate, uses easily accessible and low-cost materials for fabrication, and is applicable for implementation on a larger scale.

We proceeded to functionalize the anisotropic property of the acoustic device unit by developing two configurations of four-unit device arrays for tunable acoustic beam formation and tunable near-field focusing, respectively. We utilized the symmetry of the apertures and their capability for acoustic wave steering to form acoustic beams and foci through constructive interference.

For the first PAR configuration where the apertures were adjacent and forming edges of square, we showed controllable acoustic attenuation. A shift of the rods by decrements of 0.1 mm toward the center of the apertures could attenuate the transmitting absolute acoustic pressure by 26.3 ± 3.66 Pa. For the second PER configuration, with the apertures forming part of a “plus” shape, we showed controllable focusing and thus enhancement of the acoustic output. A shift of the rods by decrements of 0.25 mm toward the center of the apertures could increase the absolute acoustic pressure by amounts of 235.7 ± 23.79 Pa, based on the pressure peaks of the recorded focal points. Even beyond the near-field, the acoustic output for the covered apertures was greater than the case when the apertures were fully uncovered. With the ability for tunable sound attenuation and sound enhancement, creating larger arrays of apertures encompassing various rod orientations could enable more complex acoustic applications such as tunable holography. Furthermore, the second PER configuration generated focal points with an output sound pressure greater than 2000 Pa, which is within the appropriate pressure range for applications such as acoustophoretic levitation, holography, or tweezing.^[49]

Our experimental demonstrations used permanent magnets for actuation with the use of a wire and rod extension. The permanent magnet therefore controlled the rod from the side and did not obstruct the acoustic wave propagation path. An additional benefit of our method was the allowance for tilted or upside-down operation. The permanent magnet and magnetic properties of the rod ensured that the rod would not slip or fall off the substrate. The use of magnetic actuation with magnetorheological elastomers^[41,42] showed how our design could be integrated with soft robotics techniques. In addition, magnetorheological elastomers could be fabricated using the alignment of magnetic particles, which was not implemented in this work. Magnetic alignment could be beneficial to improve the precision of the actuation due to the anisotropy of the magnetic material itself,^[50] which could allow control of different parts of the rod (or any other shape), to allow motions such as rotation. The magnetorheological elastomers and magnetic actuation mechanisms have also been utilized for developing various elastic and mechanical magnetic materials and devices,^[51] where implementation of magnetic field effects in the finite element model of the coupled system has been realized.

From the perspective of sound manipulation, our “rod and aperture” mechanism is compatible with other actuation methods, without compromising the basic functionalities. This makes it a versatile design. However, there are limitations to the current setup which is magnetically controlled by permanent magnets. This method is suitable for controlling a single, or few apertures, but it would be challenging to implement for multiple arrays of apertures. In an array, the use of permanent magnets would limit the proximity of the apertures as the magnets would be attracted to one another, and it would be difficult to move them in a small space. The actuation, as well as the scope and complexity of functionalities, could be improved with alternative actuation methods such as with electromagnets, fluidic forces, or mechanical mechanisms for automation and large-scale control.

This research opens a new pathway to explore acoustically anisotropic device design properties for future applications. The shape, radius, curvature, and length of the obstacle

(e.g., rod, cube, or cone) could be explored along with different aperture dimensions based on different wavelengths to obtain unique sound behavior. Moreover, instead of a rectangular profile, the apertures could be asymmetrical, circular, hexagonal, or even a combination of shapes. In the simulated arrays, the rods were all moved at the same time. Future exploration could involve more diverse patterns of rod orientations, aperture coverage, and aperture locations. Furthermore, as our acoustic device is scalable to lower frequencies, apertures and rods of different sizes could possibly be combined together for tunable broadband acoustic operation, which would be especially useful for future commercial sound applications. Our tunable aperture-based design possesses the capability to be expanded and to bolster tangible implementations in real-world scenarios.

5. Experimental Section

Fabrication Methods: We used a transparent and thin ($0.2\text{ mm} \approx \lambda/43$ height) PET substrate. The aperture, with a width of 0.5 mm and length of 4.5 mm , was laser-cut into the PET using a VLS 2.30 ($100\text{ }\mu\text{m}$ resolution) laser cutter. We hand-mixed micron-sized ($<5\text{ }\mu\text{m}$) magnetite particles with Ecoflex 00-30 in a 1:1 ratio. Afterward, the mixture was dispensed within a piece of polyvinyl chloride tubing, with a diameter of 2 mm . The tube was used as a mold for the magnetic silicone. After 3–4 h, the cured rod was removed from the mold. The length of the casted rod was cut to be 8 mm . We actuated the magnetic silicone cylindrical rod by actuating another attached smaller magnetic cylinder (which we called rod extension) on one end using a neodymium magnet ($\approx 0.3\text{ T}$).

Transmission Measurements: In the experimental setup (Figure 1a), we placed the ultrasonic transducer (Murata, MA40S4S) directly below the substrate to emit 40 kHz waves normally incident to the aperture. The transducer was driven at a sinusoidal input voltage of 20 V_{pp} . A receiver scanned the surrounding measurement area in three orthogonal planes, YZ, XZ, and XY, with a scan area of $50\text{ mm} \times 50\text{ mm}$. Here, the receiver was a Brüel & Kjær 4138-a-015 microphone that was attached to a CNC machine arm for scanning. A Brüel & Kjær 2670 preamplifier was used with the microphone, which was externally polarized. The signals were stored digitally through a PicoScope 4262 for analysis to obtain the amplitude and phase of transmitting sound waves.

Numerical Simulations: We used the COMSOL Multiphysics, Version 6.1, pressure acoustics module to carry out 3D numerical simulations of the acoustic wave field for the solid–air interface of the rod and aperture. Both the PET substrate and rod contributed to the high impedance contrast with the air. We modeled a 3D spherical geometry of air (50 mm radius), and a PML (5 mm) was modeled on the boundary of the spherical domain. The metamaterial and transducer were placed within the boundary of the spherical domain to avoid unwanted interference and reflections. The ultrasound dynamics were visualized using the “pressure acoustics, frequency domain” module. The sound waves propagation data were captured by defining slices in different orthogonal planes for further postprocessing, and further analysis and plotting were done using MATLAB software.

Supporting Information

Supporting Information is available from the Wiley Online Library or from the author.

Acknowledgements

This work was supported by the EU-H2020 through their ERC Advanced Grant (grant no. 787413) and the Royal Academy of Engineering through their Chairs in Emerging Technology Program (grant no. CIET 17/18).

The authors acknowledge Ms. Ana Marques for her help in making the schematics for this work.

Conflict of Interest

The authors declare no conflict of interest.

Data Availability Statement

The data that support the findings of this study are available from the corresponding author upon reasonable request.

Keywords

acoustic devices, magnetic actuation, sound wave manipulation, tunable apertures

Received: August 24, 2023

Revised: January 7, 2024

Published online: January 29, 2024

- [1] L. Zhao, E. Laredo, O. Ryan, A. Yazdkhasti, H. T. Kim, R. Ganye, T. Horiuchi, M. Yu, *Appl. Phys. Lett.* **2019**, *116*, 7.
- [2] J. Hardwick, B. Kazemi, M. S. Talamali, G. Christopoulos, S. Subramanian, *Adv. Mater. Technol.* **2023**, 2301459, <https://doi.org/10.1002/admt.202301459>.
- [3] C. Choi, S. Bansal, J. Hardwick, N. Münzenrieder, M. K. Tiwari, S. Subramanian, *Commun. Mater.* **2024**, *5*, 3.
- [4] S. Bansal, S. Subramanian, *Adv. Mater. Technol.* **2021**, *6*, 2100491.
- [5] C. Hou, Z. Li, C. Fei, Y. Li, Y. Wang, T. Zhao, Y. Quan, D. Chen, X. Li, W. Bao, Y. Yang, *Commun. Phys.* **2023**, *6*, 252.
- [6] R. Hirayama, D. Martinez Plasencia, N. Masuda, S. Subramanian, *Nature* **2019**, *575*, 320.
- [7] M. Moghaddaszadeh, R. Adlakha, M. A. Attarzadeh, A. Aref, M. Nouh, *Phys. Rev. Appl.* **2021**, *16*, 034033.
- [8] R. Adlakha, M. Nouh, *Smart Mater. Struct.* **2023**, *32*, 074001.
- [9] F. Zangeneh-Nejad, R. Fleury, *Rev. Phys.* **2019**, *4*, 100031.
- [10] S. A. Cummer, J. Christensen, A. Alù, *Nat. Rev. Mater.* **2016**, *3*, 1.
- [11] B. I. Popa, D. Shinde, A. Konneker, S. A. Cummer, *Phys. Rev. B: Condens. Matter Mater. Phys.* **2015**, *91*, 235137.
- [12] G. Wen, S. Zhang, H. Wang, Z. P. Wang, J. He, Z. Chen, J. Liu, Y. M. Xie, *Int. J. Mech. Sci.* **2023**, *239*, 107872.
- [13] Z. Wang, C. Zhang, X. Li, *AIP Adv.* **2022**, *12*, 065114.
- [14] B. Assouar, B. Liang, Y. Wu, Y. Li, J. C. Cheng, Y. Jing, *Nat. Rev. Mater.* **2018**, *3*, 460.
- [15] A. Arjunan, A. Baroutaji, J. Robinson, *Encycl. Smart Mater.* **2022**, *3*, 1.
- [16] G. Liao, C. Luan, Z. Wang, J. Liu, X. Yao, J. Fu, *Adv. Mater. Technol.* **2021**, *6*, 2000787.
- [17] S. Bansal, C. Choi, J. Hardwick, B. Bagchi, M. K. Tiwari, S. Subramanian, *Adv. Eng. Mater.* **2023**, *25*, 2201117.
- [18] G. Ma, P. Sheng, *Sci. Adv.* **2016**, *2*, 1501595.
- [19] C. Choi, S. Bansal, N. Münzenrieder, S. Subramanian, *Adv. Eng. Mater.* **2020**, *2*, 2000988.
- [20] G. Memoli, M. Caleap, M. Asakawa, D. R. Sahoo, B. W. Drinkwater, S. Subramanian, *Nat. Commun.* **2017**, *8*, 14608.
- [21] Y. Wang, Y. Cheng, X. Liu, *Sci. Rep.* **2019**, *9*, 7301.
- [22] Y. Li, M. B. Assouar, *Sci. Rep.* **2015**, *5*, 17612.
- [23] X. Jiang, Y. Li, B. Liang, J. Cheng, L. Zhang, *Phys. Rev. Lett.* **2016**, *117*, 034301.

- [24] Y. Li, X. Jiang, B. Liang, J. Cheng, L. Zhang, *Phys. Rev. Appl.* **2015**, *4*, 024003.
- [25] Y. Li, S. Qi, M. B. Assouar, *New J. Phys.* **2016**, *18*, 043024.
- [26] R. Al Jahdali, Y. Wu, *Appl. Phys. Lett.* **2016**, *108*, 031902.
- [27] J. Mei, Y. Wu, *New J. Phys.* **2014**, *16*, 123007.
- [28] M. A. Norasikin, D. M. Plasencia, S. Polychronopoulos, G. Memoli, Y. Tokuda, S. Subramanian, in *UIST 2018 - Proc. 31st Annual ACM Symp. User Interface Software and Technology*, Berlin, Germany, October **2018**, p. 247.
- [29] M. H. Lu, X. K. Liu, L. Feng, J. Li, C. P. Huang, Y. F. Chen, Y. Y. Zhu, S. N. Zhu, N. Ben Ming, *Phys. Rev. Lett.* **2007**, *99*, 098103.
- [30] J. Christensen, L. Martin-Moreno, F. J. Garcia-Vidal, *Phys. Rev. Lett.* **2008**, *101*, 014301.
- [31] J. Zhu, J. Christensen, J. Jung, L. Martin-Moreno, X. Yin, L. Fok, X. Zhang, F. J. Garcia-Vidal, *Nat. Phys.* **2011**, *7*, 52.
- [32] H. Su, X. Zhou, X. Xu, G. Hu, *J. Acoust. Soc. Am.* **2014**, *135*, 1686.
- [33] H. Estrada, P. Candelas, A. Uris, F. Belmar, F. J. García De Abajo, F. Meseguer, *Phys. Rev. Lett.* **2008**, *101*, 084302.
- [34] B. Lam, D. Shi, W. S. Gan, S. J. Elliott, M. Nishimura, *Sci. Rep.* **2020**, *10*, 1.
- [35] X. Lu, J. Twiefel, Z. Ma, T. Yu, J. Wallaschek, P. Fischer, *Adv. Sci.* **2021**, *8*, 2100888.
- [36] S. Fan, S. Zhao, L. Cao, Y. Zhu, A. Chen, Y. Wang, K. Donda, Y. Wang, B. Assouar, *Phys. Rev. B* **2020**, *101*, 024104.
- [37] J. Qian, H. X. Sun, S. Q. Yuan, X. J. Liu, *Appl. Phys. Lett.* **2019**, *114*, 013506.
- [38] J. H. Park, H. J. Lee, Y. Y. Kim, *J. Appl. Phys.* **2016**, *119*, 034901.
- [39] F. Ju, W. Xiong, C. Liu, Y. Cheng, X. Liu, *Appl. Phys. Lett.* **2020**, *114*, 113507.
- [40] W. Hu, G. Z. Lum, M. Mastrangeli, M. Sitti, *Nature* **2018**, *554*, 81.
- [41] K. Yu, N. X. Fang, G. Huang, Q. Wang, *Adv. Mater.* **2018**, *30*, 1706348.
- [42] J. Kang, M. R. Haberman, *Appl. Phys. Lett.* **2022**, *121*, 181703.
- [43] T. H. Yang, J. R. Kim, H. Jin, H. Gil, J. H. Koo, H. J. Kim, *Adv. Funct. Mater.* **2021**, *31*, 2008831.
- [44] H. Seifi, S. Chew, A. J. Nascè, W. E. Lowther, W. Frier, K. Hornbæk, in *Proc. 2023 CHI Conf. Human Factors in Computing Systems*, Hamburg, Germany, April **2023**, p. 1.
- [45] Z. Tian, C. Shen, J. Li, E. Reit, Y. Gu, H. Fu, S. A. Cummer, T. J. Huang, *Adv. Funct. Mater.* **2019**, *29*, 1808489.
- [46] S. Chen, Y. Fan, F. Yang, K. Sun, Q. Fu, J. Zheng, F. Zhang, *Front. Mater.* **2021**, *8*, 790987.
- [47] K. Sun, Y. Fan, S. Chen, F. Yang, J. Li, Q. Fu, F. Zhang, *Mater. Des.* **2022**, *224*, 111352.
- [48] B. Liang, J. C. Cheng, C. W. Qiu, *Nanophotonics* **2018**, *7*, 1191.
- [49] A. Marzo, B. W. Drinkwater, *Proc. Natl. Acad. Sci. U. S. A.* **2019**, *116*, 84.
- [50] M. Moghaddaszadeh, A. Ragonese, Y. Hu, Z. Guo, A. Aref, C. Zhou, S. Ren, M. Nouh, *Commun. Mater.* **2023**, *4*, 94.
- [51] C. D. Pierce, C. L. Willey, V. W. Chen, J. O. Hardin, J. D. Berrigan, A. T. Juhl, K. H. Matlack, *Smart Mater. Struct.* **2020**, *29*, 065004.